

Na_{1.82}K_{0.38}Rb_{0.80}Fe₃(AsO₄)₄: Synthesis, crystal structure and alkali conduction pathways simulation

Eya Rezgui¹, Amira Souilem^{1,2}, Chokri Issaoui¹, Najoua Ouerfelli^{1,*} and Mohamed Faouzi Zid¹

¹Laboratory of Materials, Crystallochemistry and Applied Thermodynamics, Faculty of Sciences of Tunis, University of Tunis El Manar, Tunisia

²Chemistry Department, Faculty of Sciences and Humanities in Afif, Shaqra University, 11921 Afif, Saudi Arabia.

*E-mail: najouerf@yahoo.fr

Received: 7 January 2020 / Accepted: 2 March 2020 / Published: 10 May 2020

A new iron arsenate Na_{1.82}K_{0.38}Rb_{0.80}Fe₃(AsO₄)₄ (**1**), with layer structure has been synthesized by solid-state method and studied by X-ray diffraction. It crystallizes in orthorhombic space group Cmce with lattice parameters a=10.8710(9)Å, b=20.882(2)Å, c=6.5163(7)Å, V= 1479.3(2)Å³ and Z = 4. The final agreement factors are R = 0.039 and wR = 0.109. The X-ray single-crystal structure reveals a layered structure. Each layer is made of AsO₄ tetrahedra and FeO₆ octahedra sharing corners and edges. The Rb⁺ and K⁺ reside between the undulating iron arsenate slabs, whereas the smaller Na⁺ cations are located in the cavities of the anionic framework. The structural model was validated by bond valence sum (BVS), distortion indices (DI) and charge distribution (CD) methods. Pathways migration simulation of alkali cations was studied by extended BVS models (BVSP and BVEL).

Keywords: Iron arsenate, Crystal structure, Bond valence analysis, Pathways simulation, Ionic conductor.

1. INTRODUCTION

The search of new inorganic materials with open frames two- or three-dimensional is currently a field of intensive activity because of their widespread applications in ion-exchange [1], ionic conductivity [2,3] and catalysis [4]. In this respect, we are interested in materials with the general formula A^I₃M^{III}₃(XO₄)₄ (A^I = alkali ions, M^{III} = trivalent cations and X = P or As). One of the important applications of this family is lithium battery materials either primary (non-rechargeable) or secondary (rechargeable) [5].

Investigation of this family, except for some compounds, shows that all compounds exhibit layered structures pretty similar to $\text{K}_3\text{Fe}_3(\text{PO}_4)_4 \cdot \text{H}_2\text{O}$ [6]. Until now, four different structure types are known: two orthorhombic and two monoclinic types and will be discussed in the next few lines.

In the orthorhombic system ($a \sim 10.6\text{\AA}$, $b \sim 20.8\text{\AA}$ and $c \sim 6.5\text{\AA}$), $\text{K}_3\text{Fe}_3(\text{PO}_4)_4 \cdot \text{H}_2\text{O}$ [6] is the first hydrate synthesized compound. It crystallizes in space group $Pnma$. All the arsenates ($\text{K}_3\text{Cr}_3(\text{AsO}_4)_4$ [7], $\text{K}_3\text{Fe}_3(\text{AsO}_4)_4$ [8], $\text{K}_{1.8}\text{Sr}_{0.6}\text{Al}_3(\text{AsO}_4)_4$ [9], $\text{Na}_2\text{KAl}_3(\text{AsO}_4)_4$ [10], $\text{Na}_{1.67}\text{K}_{1.33}\text{Al}_3(\text{AsO}_4)_4$ [11] and $\text{Na}_{2.77}\text{K}_{1.52}\text{Fe}_{2.57}(\text{AsO}_4)_4$ [12] and only one phosphate $\text{K}_3\text{Cr}_3(\text{PO}_4)_4$ [13], crystallize in space group $Cmce$.

In the monoclinic system, $\text{Na}_3\text{Fe}_3(\text{PO}_4)_4$ [14] and $\text{Cs}_3\text{In}_3(\text{PO}_4)_4$ [15] crystallize in space group $C2/c$, and $\text{K}_3\text{In}_3(\text{PO}_4)_4$ [16] crystallizes in space group $P2_1/n$ (It is noted that only alkaline indium phosphates of this family have a three dimensional framework with tunnels).

As a result of further investigation of this crystal family, we present here the synthesis and characterization by single crystal X-ray diffraction of the novel $\text{Na}_{1.82}\text{K}_{0.38}\text{Rb}_{0.80}\text{Fe}_3(\text{AsO}_4)_4$ arsenate.

Following a more in-depth study of this family, synthesis and characterization by X-ray diffraction have been performed on a single crystal of the new arsenate $\text{Na}_{1.82}\text{K}_{0.38}\text{Rb}_{0.80}\text{Fe}_3(\text{AsO}_4)_4$.

The obtained structural model (1) was investigated by means of bond valence sum (BVS) [17-18] and by charge distribution (CHARDI) [19-20] analysis. To predict the electrical properties, alkali ion transport pathways were simulated using an extension of the BVS model. [12, 21-22].

2. EXPERIMENTAL

2.1. Synthesis and characterisation

Single crystals of $\text{Na}_{1.82}\text{K}_{0.38}\text{Rb}_{0.80}\text{Fe}_3(\text{AsO}_4)_4$ were prepared from a mixture of Na_2CO_3 , K_2CO_3 , Rb_2CO_3 , $\text{Fe}(\text{NO}_3)_3 \cdot 9\text{H}_2\text{O}$, and $\text{NH}_4\text{H}_2\text{AsO}_4$ with the molar ratio of $\text{Na}:\text{K}:\text{Rb}:\text{Fe}:\text{As} = 1.5:1:0.5:6:4$. First, the mixture was ground and heated in an alumina crucible at 673 K in air for 12 h in order to separate volatile products. Then, the resulting mixtures were heated slowly up to 1013K for one week to enhance the crystals growth. Lastly, the product was gradually cooled to 773 K at 5 K h^{-1} to promote crystal growth then furnace cooled to room temperature. The light green-colored crystals were retrieved upon washing with deionised water.

A qualitative analysis by energy dispersive x-ray spectroscopy (EDX) revealed the presence of Na, K, Rb, Fe, As and oxygen elements. The micrographs of these crystals are given in figure1, however the formula of the compound $\text{Na}_{1.82}\text{K}_{0.38}\text{Rb}_{0.80}\text{Fe}_3(\text{AsO}_4)_4$ has been determined as a result of crystal structure.

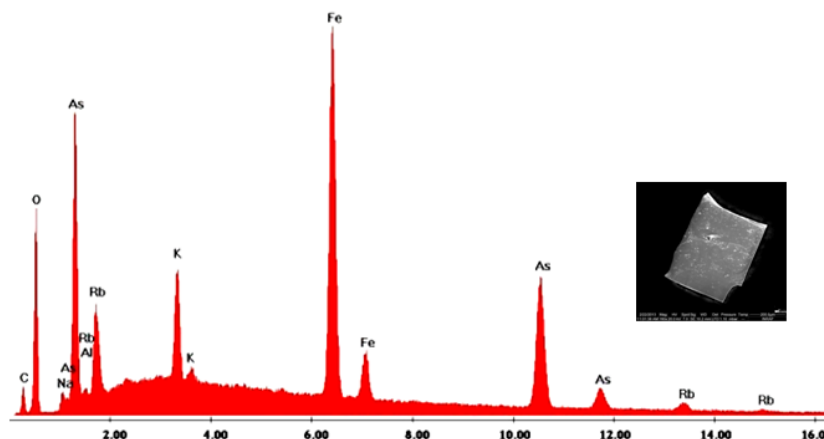


Figure 1. EDS spectrum and SEM micrograph (inset of the figure) of **1**.

2.2. X-ray data collection and structure refinement

Light green plate crystals were selected under an optical microscope equipped with a polarized light attachment and mounted on glass fiber for the structure determination and refinement. The data collections were carried out at room temperature using a four-circle Enraf-Nonius CAD-4 [23,24] diffractometer equipped with a graphite monochromator of Mo K_{α} radiation ($\lambda = 0.71073 \text{ \AA}$) (ω - 2θ scan). The reflections were corrected for Lorentz and polarization effects and secondary extinction [25]. The absorption correction was obtained via psi-scan [26]. The crystal structure was solved by direct methods and refined against F^2 in the space group $Cmce$ using the SHELX97 computer programs [25] included in the WingX software package [27]. The presence of both alkali cations (Na^+ , K^+ and Rb^+) in crystal structure is confirmed by the semi-quantitative energy-dispersive spectroscopy (EDS) analysis (Fig. 1). Iron, arsenate, alkali atoms were first located and then oxygen atoms were found by successive Fourier difference synthesis. The agreement factors R and wR were converged to 0.039 and 0.109, respectively.

The crystallographic data for title compound are summarized in Table 1. The atomic coordinates, fractional occupancies and isotropic thermal factors atomic and selected bond distances are given in Tables 2 and 3, respectively. The structure graphs were designed with Diamond 2.1 via Crystal Impact [28].

Table 1. Crystal data and structure refinement for (**1**).

<i>Crystal data</i>	
Empirical formula	$\text{Na}_{1.82}\text{K}_{0.38}\text{Rb}_{0.80}\text{Fe}_3(\text{AsO}_4)_4$
Crystal system; Space group	Orthorhombic; $Cmce$
Unit cell dimensions (\AA)	$a=10.8710(9)$; $b= 20.882(2)$; $c= 6.5163(7)$
Formula weight; Density ρ_{cal}	843.31 gmol^{-1} ; $3.809 \text{ g}\cdot\text{cm}^{-3}$
V (\AA^3), Z	$1479.3(2)$; 4
Temperature, K	298(2)
Radiation; λ , (\AA)	Mo K_{α} ; 0.71073
Crystal size (mm)	$0.18 \times 0.08 \times 0.02$

Crystal color; Shape	Light green, Plate
μ , mm ⁻¹	14.65
Data collection	
Diffractometer	Enraf-Nonius CAD-4
Scan mode	$\omega/2\theta$
θ range of data collection, deg	3.69 - 26.96
Limiting indices h, k, l	-13 ≤ h ≤ 13 -1 ≤ k ≤ 26 -8 ≤ l ≤ 4
Number of reflections: measured/independent	2673/851 [$R_{\text{int}}=0.054$]
Number of reflections with $I \geq 2\sigma(I)$	807
Absorption correction; $T_{\text{min}}, T_{\text{max}}$	ψ scan; 0.367/ 0.997
Refinement	
Refinement method	Full-matrix least-squares on F^2
Parameters/Restraints	84/0
$R(F^2)$; $wR(F^2)$	0.039; 0.109
Goodness-of-Fit on F^2	1.17
$\Delta\rho_{\text{min}}, \Delta\rho_{\text{max}}$ e/Å ³	-1.99 / 1.03

Table 2. Atomic coordinates and equivalent displacement parameters (Å²) for **1**.

Atom	Wyck	x	y	z	U _{eq} [*] , Å ²	Occ. (<1)
As1	8 <i>f</i>	0.0000	0.15679 (4)	0.06537 (14)	0.0098 (3)	
As2	8 <i>e</i>	0.2500	-0.04515 (4)	0.2500	0.0079 (3)	
Fe1	4 <i>a</i>	0.0000	0.0000	0.0000	0.0114 (4)	
Fe2	8 <i>e</i>	0.2500	0.09314 (6)	0.2500	0.0094 (3)	
O1	8 <i>f</i>	0.0000	0.0884 (3)	-0.0768 (10)	0.0143 (13)	
O2	16 <i>g</i>	0.1380 (4)	0.01152 (19)	0.2074 (6)	0.0103 (8)	
O3	16 <i>g</i>	0.2125 (4)	-0.0906 (2)	0.4482 (7)	0.0123 (8)	
O4	16 <i>g</i>	0.1225 (4)	0.1553 (2)	0.2261 (7)	0.0143 (9)	
O5	8 <i>f</i>	0.0000	0.2185 (3)	-0.0896 (11)	0.0215 (15)	
Rb1	16 <i>g</i>	0.2129 (4)	0.27539 (17)	0.1227 (7)	0.0315 (9)	0.20
K1	8 <i>e</i>	0.2500	0.274 (3)	0.2500	0.19 (3)*	0.19
Na1	8 <i>f</i>	0.0000	0.1651 (4)	-0.4415 (11)	0.032 (2)	0.64
Na2	8 <i>f</i>	0.0000	0.056 (2)	-0.474 (6)	0.049 (8)*	0.17
Na3	16 <i>g</i>	-0.073 (5)	0.183 (3)	-0.415 (8)	0.013 (10)*	0.05

*U_{eq} is defined as one-third of the trace of the orthogonalized U_{ij} tensor.

Table 3. Interatomic distances (Å) in the structure for **1**.

As1 tetrahedron		As2 tetrahedron	
As1—O5	1.638 (7)	As2—O3 ^v	1.654 (4)
As1—O4	1.695 (4)	As2—O3	1.654 (4)
As1—O4 ⁱ	1.695 (4)	As2—O2 ^v	1.720 (4)

As1—O1	1.702 (6)	As2—O2	1.720 (4)
Fe1 octahedron		Fe2 octahedron	
Fe1—O1	1.913 (6)	Fe2—O4 ^v	1.905 (4)
Fe1—O1 ^{vi}	1.913 (6)	Fe2—O4	1.905 (4)
Fe1—O2 ^{vi}	2.033 (4)	Fe2—O3 ^{xi}	2.009 (4)
Fe1—O2	2.033 (4)	Fe2—O3 ^{xii}	2.009 (4)
Fe1—O2 ⁱ	2.033 (4)	Fe2—O2	2.113 (4)
Fe1—O2 ^x	2.033 (4)	Fe2—O2 ^v	2.113 (4)
Na1 polyhedron		Na2 polyhedron	
Na1—O5	2.55 (1)	Na2—O3 ^{vi}	2.43 (1)
Na1—O4 ^{xxi}	2.551 (8)	Na2—O3 ^x	2.43 (1)
Na1—O4 ^{xxii}	2.551 (8)	Na2—O1	2.68 (4)
Na1—O5 ^{xvi}	2.615 (11)	Na2—O2 ^{vi}	2.69 (3)
Na1—O3 ^{vi}	2.784 (6)	Na2—O2 ^x	2.69 (3)
Na1—O3 ^x	2.784 (6)	Na2—O2 ^{xxi}	2.72 (3)
Na1—O1	2.87 (1)	Na2—O2 ^{xxii}	2.72 (3)
Rb1 polyhedron			
Rb1—O4	2.777 (6)	Rb1—O4 ^{xviii}	3.121 (6)
Rb1—O3 ^{xvii}	2.835 (6)	Rb1—O5 ^{xix}	3.131 (6)
Rb1—O5	2.946(6)	Rb1—O4 ^{xxv}	3.234 (6)
Rb1—O5 ⁱⁱⁱ	2.981 (6)	Rb1—O4 ^{xv}	3.234 (6)
K1 polyhedron			
K1—O4	2.85 (5)	K1—O5 ^{xv}	2.916 (4)
K1—O4 ^v	2.85 (5)	K1—O3 ^{xx}	3.13 (6)
K1—O5 ⁱⁱⁱ	2.916 (4)	K1—O3 ^{xvii}	3.13 (6)
Na3 polyhedron			
Na3—O5	2.38 (5)	Na3—O4 ^{xxi}	2.47 (5)
Na3—O3 ^{vi}	2.47 (5)	Na3—O5 ^{xvi}	2.48 (5)
Symmetry codes: (i) $-x, y, z$; (ii) $x, y, z+1$; (iii) $-x, -y+1/2, z+1/2$; (iv) $x, -y+1/2, z+1/2$; (v) $-x+1/2, y, -z+1/2$; (vi) $-x, -y, -z$; (vii) $-x+1/2, -y, z+1/2$; (viii) $x, y-1/2, -z+1/2$; (ix) $-x+1/2, y-1/2, z$; (x) $x, -y, -z$; (xi) $x, -y, -z+1$; (xii) $-x+1/2, -y, z-1/2$; (xiii) $x+1/2, y, -z-1/2$; (xiv) $-x, y, z+1$; (xv) $-x+1/2, -y+1/2, -z$; (xvi) $-x, -y+1/2, z-1/2$; (xvii) $x, y+1/2, -z+1/2$; (xviii) $x, -y+1/2, z-1/2$; (xix) $x+1/2, -y+1/2, -z$; (xx) $-x+1/2, y+1/2, z$; (xxi) $-x, y, z-1$; (xxii) $x, y, z-1$; (xxiii) $-x, -y, -z-1$; (xxiv) $x-1/2, -y+1/2, -z$; (xxv) $x-1/2, y, 1/2-z$; (xxvi) $x-1/2, y, 1/2-z$.			

2.3. Crystal structure validation tools

In order to validate the structural model, both Charge Distribution analysis (CHARDI) [19] and Bond Valence Sum (BVS) methods [17,18] (Table 4) were investigated using CHARDI2015 [29] and SoftBV [18] programs respectively. The dispersion factor of the cation charges ($\sigma_{\text{cat}}=0.015$) determined by CHARDI method confirms the structure. The BVS analysis reveals that the calculated valences $V(i)$ are in agreement with the oxidation numbers with global instability index [30] $GII = 0.14 \text{ v.u}$ (Both GII and σ measure the deviation of the computed valences and charges respectively from the formal oxidation number).

Table 4. CHARDI and BVS analysis of cation polyhedra in Na_{1.82}K_{0.38}Rb_{0.80}Fe₃(AsO₄)₄

Cation	q(i).sof(i)	Q(i)	q(i).V(i)	CN(i)	ECoN(i)	d _{ar} (i)	d _{med} (i)
Rb1	0.20	0.20	0.19	8	7.42	3.03	2.95
K1	0.19	0.19	0.14	6	6.23	2.97	2.95
Na1	0.64	0.63	0.50	7	6.47	2.64	2.63
Na2	0.17	0.17	0.16	7	6.91	2.62	2.57
Na3	0.05	0.05	0.04	4	4.10	2.50	2.45
As1	5.00	5.00	5.02	4	3.96	1.68	1.68
As2	5.00	5.01	5.07	4	3.94	1.69	1.68
Fe1	3.00	3.18	3.16	6	5.82	1.99	1.98
Fe2	3.00	2.92	3.06	6	5.61	2.01	1.98

Notes: q(i) = formal oxidation number; sof(i) = site occupation factor; d_{ar}(i) = arithmetic average distance; d_{med}(i) = weighted average distance; CNs = coordination number; ECoN(i) = number of effective coordination; σ = dispersion factor on cationic charges measuring the deviation of the computed charges (Q) with respect to the formal oxidation numbers; σ_{cat} = [Σi(q_i-Q_i)²/N-1]^{1/2}=0.015.

2.4 Bond valence pathway models

Empirical relationships between bond length R and bond valence S_{A-X} given by equation (1):

$$S_{A-X} = \exp\left(\frac{R_0 - R_{A-X}}{b}\right) \quad (1)$$

is widely used in crystal chemistry to identify plausible equilibrium sites for an atom in a structure as sites where the BV sum of the atom matches its oxidation state [31]. Recently a systematic adjustment of the empirical BV parameters (b and R_0 in equation (1)) was introduced to the bond softness [32]. The resulting BV parameter set, softBV [18] and the inclusion of interactions beyond the first coordination shell, permits more adequate estimates of non-equilibrium site energies. Originally the interactions between cations A and anions X were expressed in arbitrary "valence units". However, they may be also related, as demonstrated recently [33-34], to an absolute energy scale by expressing the bond valence as a Morse-type potential. In this approach, the ionic transport pathway is identified as regions of low site energy $E(A)$ given by equation (2):

$$E(A) = D_0 \left[\sum_{i=1}^N \left(\frac{S_{A-X_i} - S_{min,A-X_i}}{S_{min,A-X_i}} \right)^2 - N \right] + E_{Coulomb}(A - B) \quad (2)$$

where the second term accounts for Coulomb interactions between mobile ions and framework defined in equation 3:

$$E_{Coulomb}(A - B) = 14.4 \frac{eV}{\text{\AA}} \frac{z_A z_B}{R_{A-B}} \operatorname{erfc}\left(\frac{R_{A-B}}{\rho_0}\right) \quad (3)$$

The fractional ion charges z_A and z_B are derived from the nominal charges and principal quantum numbers by the formalism explained in [33-34]

Coulomb attraction terms are generally integrated in the Morse attraction term. The activation energy required for the migration of a cation from a site A to a site B is the difference between the site energy (B) and the site energy (A): $E_a = E(B) - E(A)$.

The Bond Valence sum Pathways BVSP calculations were performed using JUMPITER software [35]. The atoms used in our calculation are located in a sphere of radius 20 Å. A beam of size 0.06 Å and a pitch of 0.1 Å, with a mesh distance of 0.02 Å between the points of the belt, were used [36].

The Bond Valence Energy Landscape (BVEL) calculations were performed using the 3DBVSMAPPER code using Na⁺ and K⁺ as test ions and 0.1 Å resolution grid. The BVEL isosurfaces were modeled using the VESTA 3 program [37].

3. RESULTS AND DISCUSSION

3.1. Structure description and discussion

Single crystal X-ray structural of **1** is isotopic to K₃Fe₃(AsO₄)₄ [8], and it crystallizes in the orthorhombic system with space group *Cmce*. As shown in Figure 2a, the title compound exhibits a two-dimensional network formed by alternating [Fe₃As₄O₁₆]³⁺ layers parallel to the *a-c* plane. Each layer consists of corner-sharing FeO₆ octahedra that are further connected by arsenate tetrahedra through corner and edge sharing (Fig. 2b).

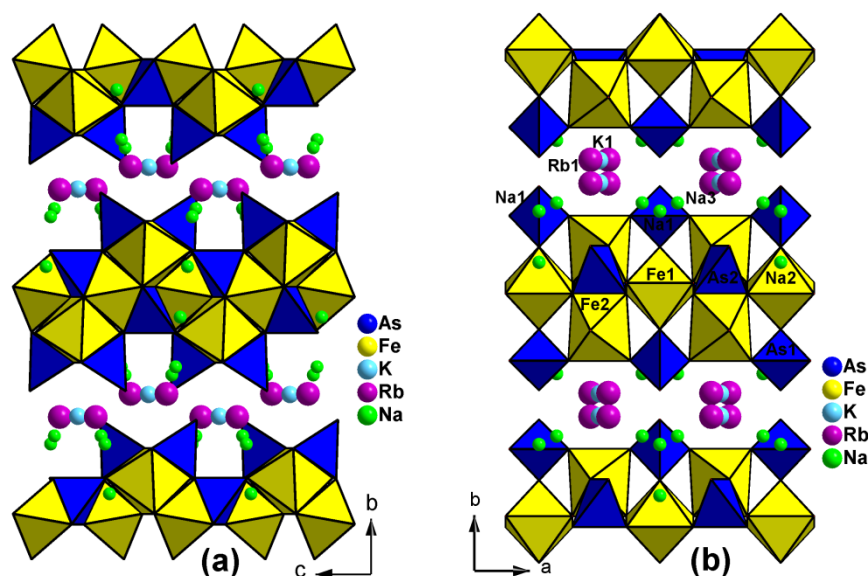


Figure 2. Projection of the **1** structure: (a) along *a* and (b) along *c* axis. (Showing the K⁺ and Rb⁺ cations reside in the interlayer space).

The K⁺ and Rb⁺ cations reside between the undulating iron arsenate layers (Fig. 2), whereas the smaller Na⁺ cations are located in the cavities of the anionic framework faces of the hexagonal sections windows (Fig. 3).

The Fe1 and Fe2 atoms are in typical octahedral coordination. The polyhedron Fe₂O₆ is slightly more distorted than Fe₁O₆, this is confirmed by the values of effective coordination numbers

(ECoN(Fe2)= 5.61 and ECoN(Fe1)= 5.82) (Table 4), and their distortion indices (*DI*) varying from 3 to 5% (Table 5).

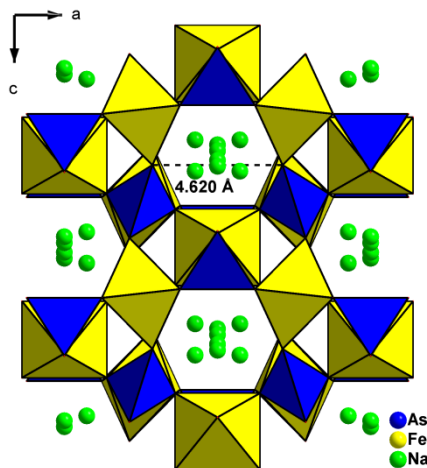


Figure 3. Layer of the (1) structure viewed along *b* axis showing the hexagonal windows.

Table 5. Distortion indices (*DI*) for the coordination polyhedra around Fe and As in $\text{Na}_{1.82}\text{K}_{0.38}\text{Rb}_{0.80}\text{Fe}_3(\text{AsO}_4)_4$

	As1	As2	Fe1	Fe2
DI_d	0.013	0.020	0.027	0.035
DI_a	0.024	0.050	0.044	0.052
DI_o	0.013	0.035	0.035	0.038
$DI_d = \sum_{i=1}^{n_1} (d_i - d_m) / n_1 d_m ; DI_a = \sum_{i=1}^{n_2} (a_i - a_m) / n_2 a_m \text{ and } DI_o = \sum_{i=1}^{n_2} (o_i - o_m) / n_2 o_m.$ <p><i>d</i>, <i>a</i> and <i>o</i> signify Fe/As-O bond distance. O-Fe/As-O angle and O-O edge within the relevant polyhedron; index <i>i</i> indicates individual values, index <i>m</i> the mean value for the polyhedron. <i>n</i>₁ and <i>n</i>₂ are 4 and 6 for the arsenate tetrahedral; 6 and 12 for the iron octahedral.</p>				

The arsenate atoms have a slightly distorted tetrahedral coordination with effective coordination numbers ECoN(As1)= 3.96 and ECoN(As2)= 3.94 (Table 4). The As–O distances vary from 1.638(7) to 1.702(6) Å and from 1.654(4) to 1.720(4) Å for As1 and As2 respectively [12]. The high values of distortion indices of As₂O₄ tetrahedron ($DI_a=5\%$ and $DI_o=4\%$) are evident. It is a result of the rigid environment surrounding As₂ (The As₂O₄ tetrahedron is edge-shared with one Fe₂O₆ octahedron).

The Na₁, Na₂ and Na₃ atoms are surrounded, respectively, by seven and four O atoms with Na–O distances varying from 2.38(5) to 2.87(1) Å. They have slightly distorted polyhedra (ECoN(Na₁)= 6.47, ECoN(Na₂)= 6.91 and ECoN(Na₃)= 4.10) (Table 4).

The rubidium ion is coordinated to eight oxygen atoms with distances ranging from 2.777(6) to 3.234(6) Å. The coordination sphere is highly asymmetrical ($\text{ECoN}(\text{Rb1})=7.42$).

K1 has an environment formed by six oxygen atoms with K–O distances at 2.85(5)-3.13(6) Å. The effective coordination number value ($\text{ECoN}(\text{K1})=6.23$) indicates that the coordination polyhedron of K1 approximates a slightly distorted octahedron.

The coordination number of the cations Rb^+ , K^+ and Na^+ was calculated on the basis of the maximum deviation of the cation-O distance; $L_{\text{max}} = 3.42\text{Å}$ for Rb-O, 3.35Å for K-O and 3.13Å for Na-O according to Donnay and Allman [38].

3.2. Pathways transport simulation proposed from bond valence analysis

3.2.1 Alkali pathways transport simulation by BVSP

In order to investigate the ionic diffusion properties, the alkali conduction pathways in the crystal bulk were simulated. These methods have been described in detail elsewhere and have been extensively used for predicting defects and ion migration. The procedure allows identifying a pathway of points with the lowest valence which correspond to the lowest energy of mobile cations in the lattice, where BVS model only considers cation-anion (O^{2-}) interactions.

The crystal structure study shows two cations: K1 and Rb1 in interlayer space (Fig. 2) and three sodium cations Na1, Na2 and Na3 (Fig. 3) in interconnected cavities along *b*-axis.

The pathway analysis suggests that the rubidium ions do not participate in the cationic mobility.

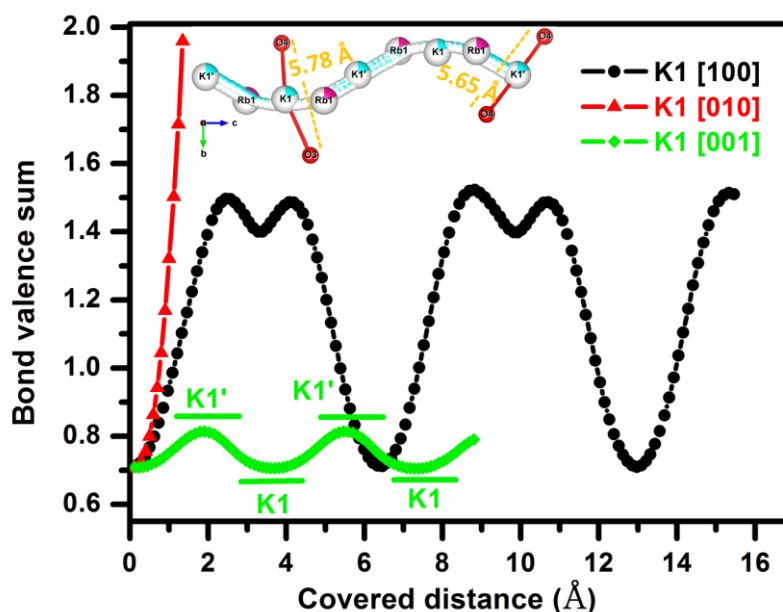


Figure 4. Bond valence sum for K1 ions versus the covered distance

The migration pathways of potassium cations for a 8.8 Å distance are one-dimensional along [001]. The zigzag form of this path is due to the alternative migration of the potassium cation in the

interlayer between the maximal distance d_{O4-O3} equal to 5.78 Å with a 0.70 u.v and the minimal distance d_{O4-O4} equal to 5.65 Å with 0.81 u.v. while the mobility of K^+ is not favorable along [100] direction since the interlayer distances vary from 4.69 Å to 5.51 Å which are inferior to 5.6 Å the sum of K^+ and O^{2-} diameters (Figs. 4-5).

The migration pathways simulation of Na^+ cations by the BVSP method along the probable directions shows:

- 1- The migration pathways of Na1 and Na3 cations in the interlayer space seemed to be one-dimensional along [100] direction (Figs. 5-6).
- 2- The Na1 cation, located at an interlayer distance equal to 4.83 Å above 0.76 u.v, reaches the closest Na3 cation. The Na1 cation migrates for 0.83 Å with 0.79 u.v. The valence unit slightly decreases due to the crystallographic position of Na3 situated at an interlayer distance equal to 4.69 Å. Then, it migrates for 3 Å distance reaching the lowest unit valence (0.42 u.v), characterized by the largest interlayer distance 5.51 Å between Rb1 and K1 crystallographic positions (Fig. 6). In fact, Na1 and Na3 cations mobility in the interlayer space along [100] direction does not exceed 0.79 u.v for 12 Å travelled distance (Figs. 5-6).

Along [010] direction, the tunnel minimum size where the Na2 cations are located is equal to 4.62 Å corresponding to 0.94 u.v (Fig. 7). Then, the sodium cation migrates for 2.31 Å distance to a larger place (4.83 Å), where Na1 cations are situated, leading to the diminution of the valence unit 0.76 u.v (Fig. 7) and (Fig. 3). However, Na3 cation with 0.93 u.v. reaches Na2 positions twice at 2.92 Å and 5.26 Å distances. Then it reaches the other position of Na3 at a 7.72 Å distance with 0.76 u.v (Fig. 7).

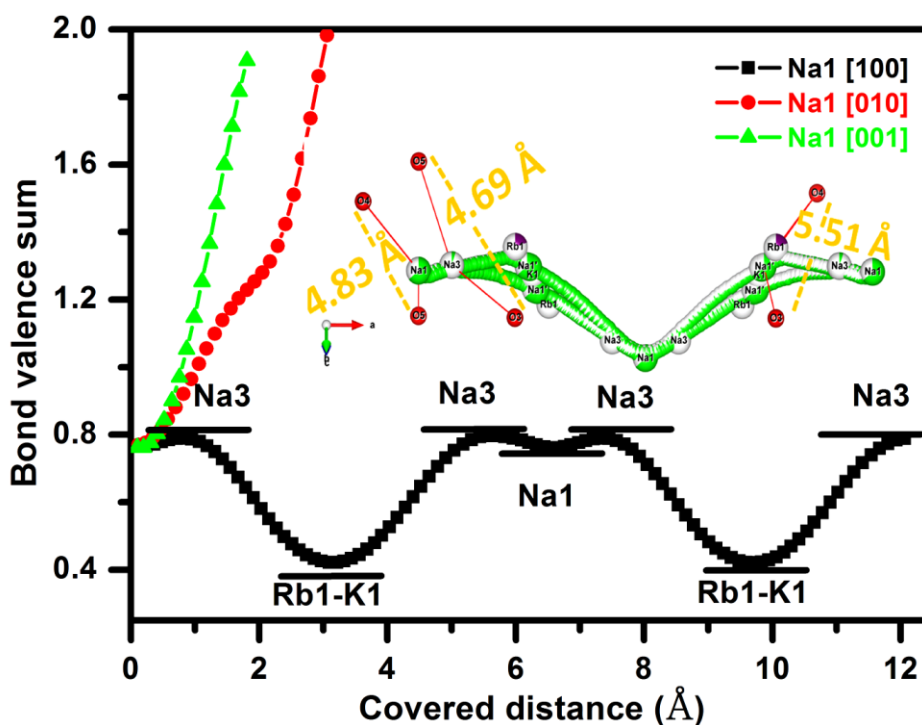


Figure 5. Bond valence sum for Na1 ions versus the covered distance.

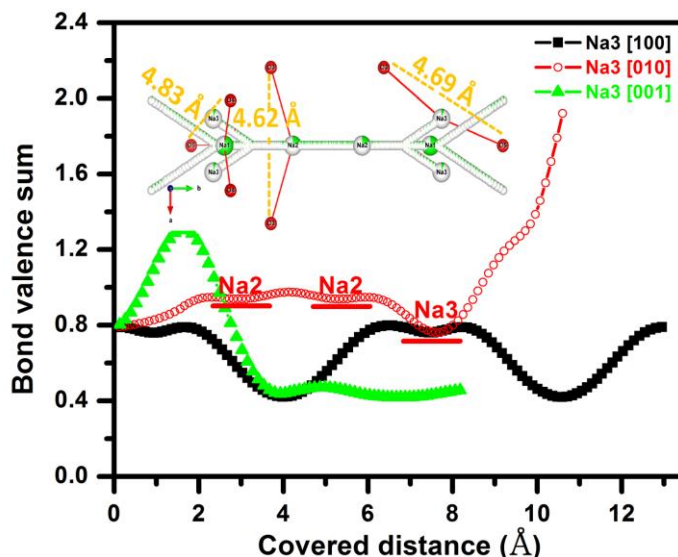


Figure 6. Bond valence sum for Na3 ions versus the covered distance.

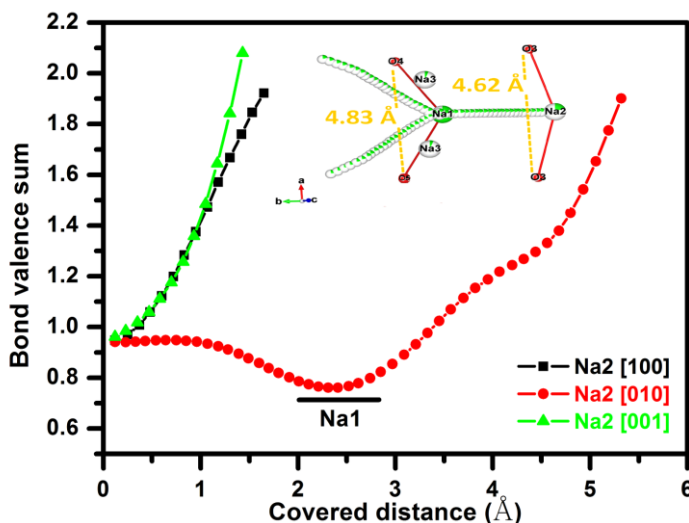


Figure 7. Bond valence sum for Na2 ions versus the covered distance.

3.2.2. Alkali pathways transport simulation by BVEL

The bond valence method was employed successfully to model ionic transport pathways [39-42]. In order to determine the 3D conduction pathways of both ions, the Bond Valence Energy Landscape (BVEL) method was investigated.

The BVEL simulation shows that potassium ions have a site energy equal to E_{min} above 4.32 eV. At an activation energy equal to $E_a = 0.40$ eV, as it was deduced from the BVSP simulation, the isosurface merges into an infinite network of conduction paths of K^+ cations that extends along the [001] direction with a zigzag form (Fig. 8).

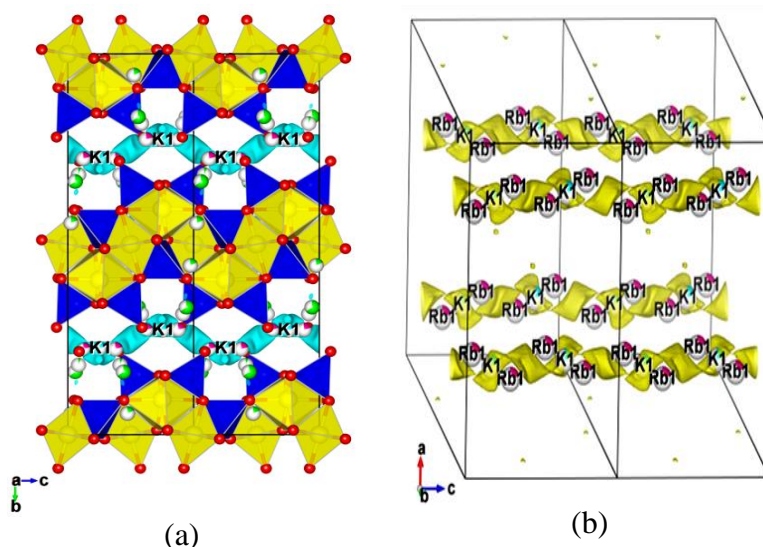


Figure 8. BVEL maps for potassium cation in $\text{Na}_{1.82}\text{K}_{0.38}\text{Rb}_{0.80}\text{Fe}_3(\text{AsO}_4)_4$ at $E_a = 0.4$ eV. **(a):** Infinite conduction pathways in **(1)** structure **(b):** Infinite conduction pathway

The BVEL simulation of sodium ions shows that Na2 cations have a site energy equal to $E_{\min} = -3.021$ eV. The migration of Na2 cations to their close neighbors requires an activation energy equal to 0.06 eV (Fig. 9a). According to the b direction, an infinite connection path Na1-[Na2-Na2]-Na1 was observed with a higher activation energy $E_a = 0.16$ eV (Fig. 9b).

At activation energy 0.39 eV a local infinite migration path [Na3-Na1-Na2-Na2-Na1-Na3] was observed (Fig. 10). The $\text{Na}_{1.82}\text{K}_{0.38}\text{Rb}_{0.80}\text{Fe}_3(\text{AsO}_4)_4$ compound have an activation energy equal to 0.96 eV permitting the migration of Na^+ cation from a local infinite migration path [Na3-Na1-Na2-Na2-Na1-Na3] to other infinite paths [Na3-Na1-Na2-Na2-Na1-Na3] in the same lattice and the neighbor lattices forming infinite isosurfaces...[Na3-Na1-Na2-Na2-Na1-Na3]-[Na3-Na1-Na2-Na2-Na1-Na3]... (Fig. 11).

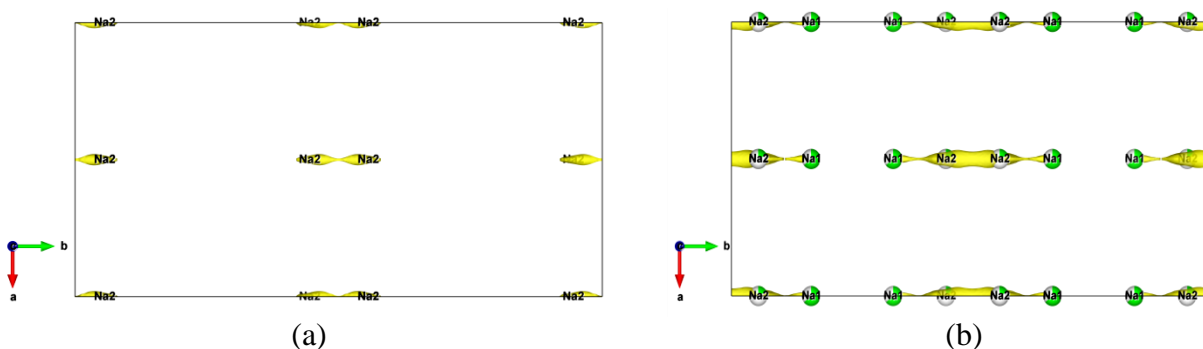


Figure 9. BVEL maps for sodium cations: **(a):** (Na2-Na2) at $E_a = 0.06$ eV, **(b):** (Na1-[Na2-Na2]-Na1) at $E_a = 0.16$ eV.

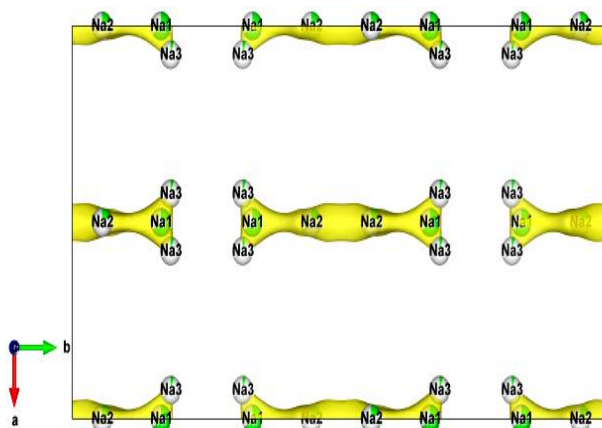


Figure 10. BVEL maps for sodium cation at $E_a = 0.39$ eV.

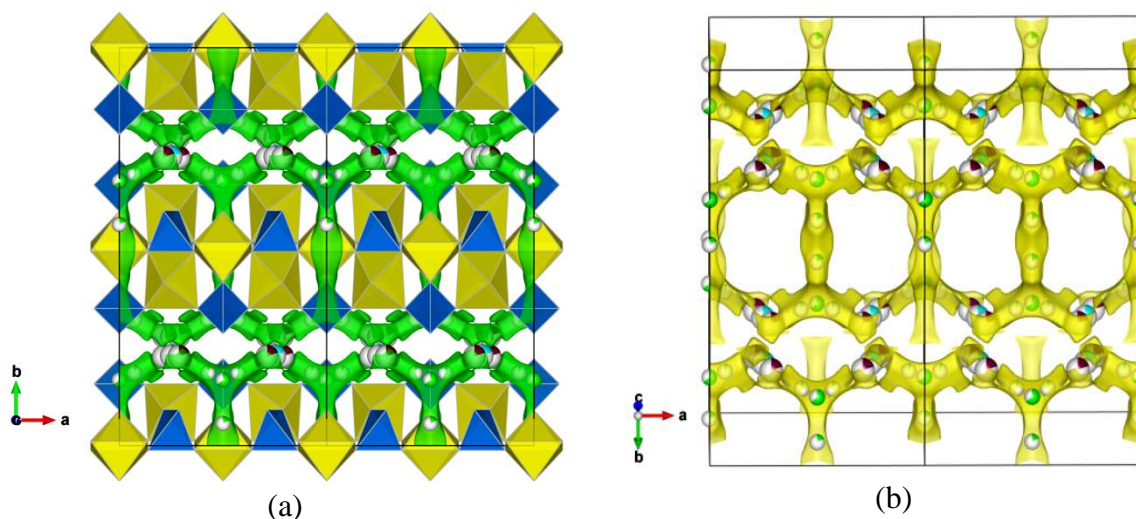


Figure 11. BVEL maps for sodium cations in $\text{Na}_{1.82}\text{K}_{0.38}\text{Rb}_{0.80}\text{Fe}_3(\text{AsO}_4)_4$ at $E_a = 0.96$ eV. (a): 3D isosurfaces in the structure, (b): Perspective 3D isosurfaces

In order to study the conduction pathways of monovalent cations by BVSP and BVEL simulation methods, a superposition of both migration routes has been investigated. At first, a total overlap between the isosurfaces calculated by BVEL and the migration paths determined by BVSP was seen, which indicates a good agreement of the two methods (Fig. 12). But if we check them more carefully, the effect of blocking the mobility of K^+ cations by Rb^+ cations according to the direction [001] (Fig. 13) and the effect of blocking the mobility of Na^+ cations by two cations K^+ and Rb^+ according to the direction [100] will appear (Fig. 14).

In the case of our material $\text{Na}_{1.82}\text{K}_{0.38}\text{Rb}_{0.80}\text{Fe}_3(\text{AsO}_4)_4$ it is probably that the large sized Rb^+ cation maintains the structure and the two other smaller K^+ and Na^+ cations migrate according to the different directions studied previously [12-36].

The theoretical activation energy calculated by the BVEL method of our compound $\text{Na}_{1.82}\text{K}_{0.38}\text{Rb}_{0.80}\text{Fe}_3(\text{AsO}_4)_4$ via the mobility of K^+ cations is equal to 0.40 eV. This energy value is very close to 0.5 eV; the experimental activation energy of its isotype $\text{Na}_{2.77}\text{K}_{1.52}\text{Fe}_{2.57}(\text{AsO}_4)_4$ [12].

Probably, we can deduce from this comparison that the K^+ cations are the most responsible for the ionic conduction of our material. Since they migrate in the interlayer space of a minimum distance equal to 5.65 Å in the direction [001]. This value is slightly greater than the sum of the two diameters of K^+ and O^{2-} (5.6 Å). While the mobility of the Na^+ cations in the interlayer space in the [100] direction and through the tunnels in the [010] direction meet bottlenecks with minimum distances successively equal to 4.69 Å and 4.62 Å. These two distance values are both less than the sum of the two diameters of Na^+ and O^{2-} which is equal to 4.82 Å.

The correlation between structural study and the simulation of the electrical properties by the BVSP and the BVEL models shows that based on the geometrical characteristics such as crystallographic sites of the cations, size and dimension and the nature of the framework favoring or not the mobility of cations, we can model the mobility of these ions by estimating the theoretical activation energy. Subsequently, we can classify our material according to their conductivity. This study allows us to detect compounds that may be good candidates for use as positive electrode materials in ion batteries. The interesting feature of $\text{Na}_{1.82}\text{K}_{0.38}\text{Rb}_{0.80}\text{Fe}_3(\text{AsO}_4)_4$ is that it has two different mobile cations (Na^+ , K^+) travelling along different directions. BVS simulations predicted the possibility for investigating this compound for battery materials. The high ion conductivity of Na^+ based electrolyte and small solvated K^+ ions are beneficial to provide a good battery performance [43].

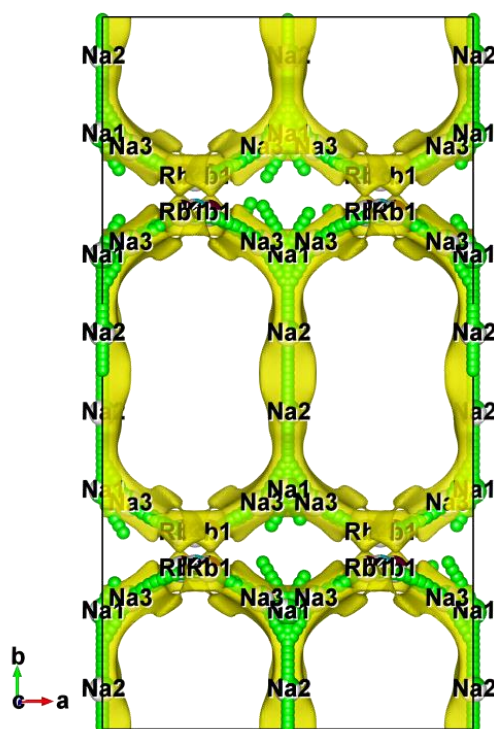


Figure 12. Superposition of calculated isosurfaces by BVEL and migration paths determined by BVSP for Na^+ cations in the (1) structure.

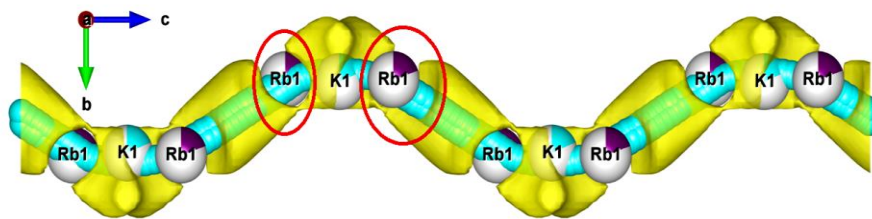


Figure 13. Superposition of calculated isosurfaces by BVEL and migration paths determined by BVSP for K^+ cations along [001] direction

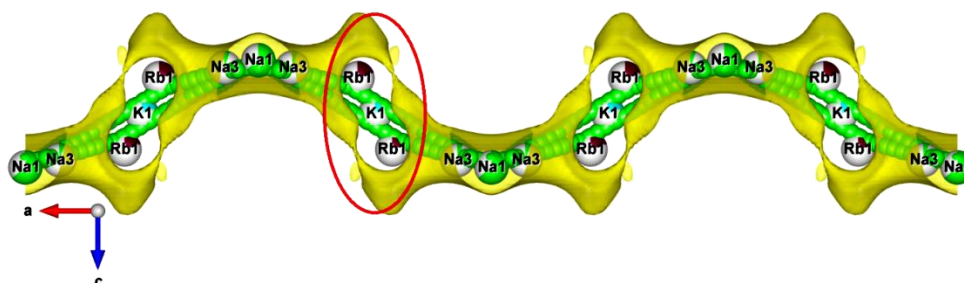


Figure 14. Superposition of calculated isosurfaces by BVEL and migration paths determined by BVSP for Na^+ cations along [100] direction.

4. CONCLUSION

A new layered iron arsenate, $Na_{1.82}K_{0.38}Rb_{0.80}Fe_3(AsO_4)_4$, was synthesized by solid state reaction. The structural formula was verified by EDX semi-quantitative elemental analysis and the crystal structure was determined by single crystal X-ray diffraction analysis. It shows a layered structure where the cations K^+ and Rb^+ reside between the undulating iron arsenate slabs, whereas the smaller Na^+ cations are located in the cavities of the anionic framework. The final structural model was validated by both bond valence sum (BVS) and charge distribution (CD) methods.

The BVS simulations were used to model the ionic migration of alkali cations in the structure. The BVSP and BVEL models show that the pathways migration of potassium in the title compound is one-dimensional along c direction. However, pathways migration of sodium is two-dimensional in a and b directions.

SUPPLEMENTARY INFORMATION

Crystallographic data for **1** has been deposited with the Cambridge Crystallographic Data Centre as supplemental publication numbers (CCDC) 1499154. Copies of the data can be obtained free of charge via <http://www.ccdc.cam.ac.uk>.

References

1. S.Y. Chung, S.Y. Choi, T.H. Kim and S. Lee, *ACS Nano*, 1 (2015) 850.

2. C.T. Hsieha, J.R. Liua, R.S. Juangb, C.E. Leea and Y.F. Chen, *Mater. Chem. Phys.*, 153 (2015) 103.
3. J.E. Garbarczyk, T.K. Pietrzak, M. Wasiucioneck, A. Kaleta, A. Dorau and J.L. Nowiński, *Solid State Ionics*, 272 (2015) 53.
4. K.P. Singh, E.J. Bae and J.S. Yu, *J. Am. Chem. Soc.*, 137 (2015) 3165.
5. K. Trad, D. Carlier, A. Wattiaux, M. Ben Amara and C. Delmas, *J. Electrochem. Soc.*, 157 (2010) A947.
6. K.H. Lii, *Eur. J. Solid State Inorg. Chem.*, 32 (1995) 917.
7. B. Bouzemi Friaa, H. Boughzala and T. Jouini, *J. Solid State Chem.*, 173 (2003) 273.
8. N. Ouerfelli, M. F. Zid and T. Jouini, *Acta Crystallogr., Sect. E: Struct. Rep. Online*, 61 (2005) 67.
9. A. Haj Abdallah and A. Haddad, *Acta Crystallogr., Sect. E: Struct. Rep. Online*, 68 (2012) i29.
10. H. Ben Yahia, T. Nilges, U. C. Rodewald, R. Pöttgen, *Mater. Res. Bull.*, 45 (2010) 2017.
11. M.A. Bouhassine and H. Boughzala, *Acta Crystallogr., Sect. E: Struct. Rep. Online*, 70 (2014) 6.
12. N. Ouerfelli, Y. Ben Smida and M.F. Zid, *J. Alloys Compd.*, 651 (2015) 616.
13. S. Kouass and H. Boughzala, *Phosphorus, Sulfur Silicon Relat. Elem.*, 181 (2006) 2641.
14. B. Lajmi, M. Hidouri, M. Rzaigui and M. Ben Amara, *Mater. Res. Bull.*, 37 (2002) 2407.
15. I.V. Zatovsky, V.N. Baumer, N.Y. Strutynska, N.S. Slobodyanik and O.V. Shishkin, *Acta Crystallogr., Sect. C: Cryst. Struct. Commun.*, 66 (2010) 71.
16. S.L. Yang, H. Zhang, Z. Xie, D. Zhao, W.L. Zhang and W.D. Cheng, *J. Solid State Chem.*, 182 (2009) 855.
17. I.D. Brown (2002) *The Chemical Bond in Inorganic Chemistry- The Bond Valence Model*. IUCR Monographs on Crystallography. 12. Oxford University Press.
18. S. Adams (2004) softBV, University of Göttingen. Germany. <http://www.softBV.net>
19. M. Nespolo, *Acta Crystallogr., Sect. B: Struct. Sci.*, 72 (2016) 51.
20. M. Nespolo, and B. Guillot., *J. Appl. Crystallogr.*, 49 (2016) 317.
21. Y. Ben Smida, R. Marzouki, A. Guesmi, S. Georges and M.F. Zid, *J. Solid State Chem.*, 221 (2015) 132.
22. Y. Ben Smida, A. Guesmi, S. Georges and M.F. Zid, *J. Solid State Chem.*, 221 (2015) 278.
23. A.J.M. Duisenberg, *J. Appl. Crystallogr.*, 25 (1992) 92.
24. J. Macíček, A. Yordanov, *J. Appl. Crystallogr.*, 25 (1992) 73.
25. G.M. Sheldrick, *Acta Crystallogr., Sect. A: Found. Crystallogr.*, 64 (2008) 112.
26. A.C.T. North, D.C. Phillips and F.S. Mathews, *Acta Crystallogr., Sect. A: Found. Crystallogr.*, 24 (1968) 351.
27. L.J. Farrugia, *J. Appl. Crystallogr.*, 32 (1999) 837.
28. K. Brandenburg and M. Berndt (2001) *Diamond Version 2.1*. Crystal Impact. Bonn.
29. M. Nespolo, (2015) CHARDT2015. A program to compute the Effective Coordination Number (ECoN) and the Charge Distribution in non-molecular crystal structures (<http://crm2.univ-lorraine.fr/lab/fr/software/chardi2015/>)
30. S. Adams, O. Moretzki and E. Canadell, *Solid State Ionics*, 168 (2004) 281.
31. I.D. Brown, *Chem. Rev.*, 109 (2009) 6858.
32. S. Adams, *Solid State Ionics* 177 (2006) 1625.
33. S. Adams and R.P. Rao, *Phys. Status Solidi A*, 208 (2011) 1746.
34. S. Adams and R.P. Rao, *Atom Indonesia*, 36 (2010) 95.
35. D. Mazza, *J. Solid State Chem.*, 156 (2001) 154.
36. I. Jendoubi, C. Issaoui and M.F. Zid, *Solid State Ionics*, 337 (2019) 178.
37. M. Sale and M. Avdeev, *J. Appl. Crystallogr.*, 45 (2012) 1054.
38. G. Donnay and R. Allmann, *Am. Mineral.*, 55 (1970) 1003.
39. S. Adams, and R.P. Rao, *J. Mater. Chem.*, 22 (2012) 76.
40. Y. Ben Smida, A. Guesmi, S. Georges and M.F. Zid, *J. Solid State Chem.*, 221 (2015) 278.
41. M. Sonni, M. F. Zid and C. Issaoui, *J. Solid State Chem.*, 272 (2019) 244.

42. M.A. Ben Moussa, R. Marzouki, A. Brahmia, S. Georges, S. Obbade and M.F. Zid, *Int. J. Electrochem. Sci.*, 14 (2019) 1500.
43. K. Kuratani, N. Uemura, H. Senoh, H. Takeshita and T. Kiyobayashi, *J. Power Sources*, 223 (2013) 175.

© 2020 The Authors. Published by ESG (www.electrochemsci.org). This article is an open access article distributed under the terms and conditions of the Creative Commons Attribution license (<http://creativecommons.org/licenses/by/4.0/>).